A high-resolution subcellular map of proteins in cells with motile cilia

*Filippa Bertilsson[1], Feria Hikmet[1], Jan N. Hansen[2,3], Mathias Uhlén[2,4], Loren Méar[1,5,6]†, Cecilia Lindskog[1]†**

†These authors contributed equally

* Corresponding author:

Cecilia Lindskog

Email: Cecilia.Lindskog@igp.uu.se

Tel: +46 18 471 50 32

[1] Department of Immunology, Genetics and Pathology, Cancer Precision Medicine Research Unit, Uppsala University, SE-75185 Uppsala, Sweden

[2] Science for Life Laboratory, School of Engineering Sciences in Chemistry, Biotechnology and Health, KTH Royal Institute of Technology, 17121 Stockholm, Sweden

[3] Department of Bioengineering, Stanford University, Stanford, CA, USA

[4] Department of Neuroscience, Karolinska Institutet, Stockholm, Sweden

[5] Department of Women's and Children's Health, Karolinska Institutet, 17177 Stockholm, Sweden

17 [6] Department of Gynecology and Reproductive Medicine, Karolinska University Hospital,
18 Stockholm, Sweden

19

20 KEYWORDS
21 Antibody-based proteomics, Human Protein Atlas, Motile cilia, Ciliated cells, multiplex
22 immunohistochemistry, image analysis, protein mapping

23

24 **Abstract**

25 Motile cilia are complex structures regulated by thousands of genes, essential for various
26 physiological functions like respiration and reproduction. Their dysfunction can result in severe
27 conditions like primary ciliary dyskinesia (PCD), highlighting the need for a deeper molecular
28 understanding of their specific ciliary compartments. Interestingly, ciliated cells harbor multiple
29 proteins with limited evidence on biological function, as defined by Functional Evidence (FE)
30 scores, a grading system developed by the Human Proteome Project (HPP). Building upon the
31 stringent antibody validation pipeline of the Human Protein Atlas (HPA) project, we developed a
32 high-throughput workflow that combines a novel multiplex immunohistochemistry protocol with
33 image analysis to investigate protein expression and subcellular localization in motile ciliated cells
34 across five human tissues: nasopharynx, bronchus, fallopian tube, endometrium, and cervix. We
35 spatially mapped >180 proteins, out of which 73% have FE scores 2-5, suggesting that further
36 evidence is needed to establish these proteins' biological function. Notably, expression patterns
37 varied between tissues, suggesting that motile cilia proteins are not universally expressed across
38 the different epithelia. Our pipeline constitutes a promising resource for comprehensive mapping

39 of the motile cilia proteome, and a first step towards identifying cilia proteins for functional studies
40 to understand the molecular mechanisms underlying ciliopathies.

41

42 **Introduction**

43 Cells are not organized randomly, but instead form complex organ systems where molecules,
44 cellular compartments and cell types are spatially distributed based on cellular function. Proteins
45 often execute their functions in specific subcellular locations, which is crucial for maintaining
46 various cellular processes such as cell growth, motility, and signaling[1]. To investigate the role of
47 proteins and their biochemical functions within the cell, knowledge about the spatial localization
48 from both a cellular and subcellular perspective is a crucial first step for further functional studies[2].

49 The Human Proteome Project (HPP) is an initiative of the Human Proteome Organization (HUPO)
50 that has contributed to credibly identifying at least one major isoform of all human proteins, mainly
51 using mass spectrometry-based methods[3]. As a next step, the HPP consortium currently leads a
52 major effort called the "Grand Challenge", with the ultimate goal to gain a solid understanding of
53 at least one biological function for each protein at the molecular level. A Functional Evidence (FE)
54 scoring system has been developed, with FE1-5 elucidating the amount of evidence for protein
55 function. The scoring system is linked to annotations contained in UniProt[4], including Gene
56 Ontology terms, publications and computational predictions where FE1 represent proteins with at
57 least one known molecular function based on experimental evidence. FE5 represents the lowest
58 scoring, indicating that basically nothing is known about the role of these proteins in human cells.
59 Interestingly, only 5,229 proteins encoded by the human genome currently have FE1, highlighting
60 the importance of further efforts that can contribute to understanding protein function.

61 With the goal of mapping all human proteins, the Human Protein Atlas (HPA) project has built
62 one of the world's largest biological knowledge resources, available as an open-access database
63 (www.proteinatlas.org). The HPA integrates both transcriptomics data and spatial antibody-based
64 proteomics[5], and within this effort, >15,000 proteins have been mapped to all major human normal
65 and cancer tissues using classical immunohistochemistry (IHC). The resource of more than 10
66 million manually annotated high-resolution histological images provides important information on
67 spatial expression patterns of proteins from a body-wide and cell type-specific perspective, but the
68 possibilities to distinguish subcellular patterns are limited.

69 Standard IHC is primarily used to study one protein per tissue section, but an increasing number
70 of methods utilize multiplexed IHC (mIHC), enabling novel insights into co-expression and tissue
71 or cell type heterogeneity. Spatial proteomics technologies are of utmost importance to
72 characterize the intrinsic subcellular functions of human proteins[6], as has been demonstrated in
73 multiple large-scale studies[2,7]. To increase the resolution of the Tissue resource, the HPA version
74 24 and onwards includes data based on a novel mIHC protocol employing in-house generated 6-
75 plex antibody panels. Using an iterative fluorescence-based staining-stripping method, fixed
76 antibody panels of five markers outlining specific cell types, cell states or subcellular structures
77 were stained together with proteins of interest. By examining overlap in expression, this workflow
78 allows for exploring protein localization in structures that are challenging to distinguish based on
79 histological examination only. This facilitates automated image analysis efforts, and minimizes
80 the subjectivity introduced during manual annotation[7,8].

81 Interestingly, when comparing the FE scores with single cell type specificity in the HPA, a dataset
82 based on single-cell transcriptomics[9], as many as 441 proteins with FE2-5 showed an elevated
83 expression in ciliated cells. This suggests that further mapping of these cells is an important

84 contribution towards understanding protein function. Here, we therefore seek to further explore
85 the cilium (plural cilia), a filamentous hair-like cellular membrane protrusion, whose assembly
86 (ciliogenesis) and structure requires at least 2,000 genes[10]. Cilia are canonically distinguished into
87 two types: primary cilia and motile cilia. Motile cilia are present on epithelia of different organs
88 where they aid in transporting cells, fluids, particles or mucus, and are crucial for e.g. reproduction,
89 respiration, L/R body asymmetry, or brain development and function[11]. Defects in genes related
90 to motile cilia have been linked to motile ciliopathies, contributing to a large spectrum of diseases
91 in various tissues, including chronic respiratory problems, infertility, and hydrocephalus[12]. The
92 most common ciliopathy, primary ciliary dyskinesia (PCD), is characterized by impaired ciliary
93 movement. PCD is usually caused by autosomal recessive mutations, but also by autosomal
94 dominant and even X-linked mutations in rare cases[13,14].

95 Despite advancements in understanding PCD in the last 20 years, its diagnosis remains
96 challenging, and effective treatments are lacking[15]. Studying motile cilia genes can provide us with
97 fundamental insights into ciliary function and structure, being a first step towards understanding
98 the underlying molecular mechanisms of ciliopathies (e.g., impaired mucociliary clearance in the
99 airways)[16]. Structurally, the cilium comprises several distinct regions: the basal body, containing
100 a modified centriole anchoring the cilium to the cell; the ciliary rootlet, a fibrous structure
101 anchoring the basal body to the cell and it's cytoskeleton for additional support; the transition zone,
102 a specialized gateway at the ciliary base (between basal body and cilium) that regulates protein
103 trafficking and acts as a diffusion barrier; and the axoneme, the core ciliary skeleton that extends
104 from the basal body, traverses the transition zone and that is composed of microtubule doublets
105 and associated motor proteins that mediate ciliary movement[11,17]. Given their small size, close
106 spatial proximity, and dynamic nature, these compartments are best studied for their architecture

using imaging and microscopy-based methods[18]. While electron microscopy and Cryo-ET have been instrumental in profiling ciliary ultrastructure, these techniques primarily reveal stable structural components like the axoneme, basal body, and transition zone, but often fail to preserve and visualize soluble or transiently associated proteins. Non-structural proteins yet remain underrepresented in structural studies. To our knowledge, no previous mIHC approach exists that enables comprehensive characterization of both structural and non-structural proteins in the different sub-compartments of ciliated cells at a high resolution. Therefore, we developed a medium-plex mIHC panel specifically designed to map cells with motile cilia.

With this background, the aim of the study was to develop a novel high-throughput workflow for quantifying cilia proteins at subcellular resolution using mIHC and automated image analysis, a first step towards understanding protein function. Based on signal overlap with a panel of marker proteins outlining the cilium, the transition zone, the rootlet, the cytoplasm, and the nucleus of ciliated cells, the spatial subcellular localization of 187 motile cilia proteins was mapped across five different tissue types from both respiratory (nasopharynx and bronchus) and reproductive tracts (fallopian tube, endometrium and cervix). The detailed information at the tissue, cellular, and subcellular levels offered new insights into the presumed functions of these proteins in motile cilia. Moreover, our approach, combining spatial proteomics with automated image analysis enables detailed spatial mapping at the subcellular level, offering a valuable resource for future large-scale studies of cilia biology in health and disease. The resulting images can be explored in the open access Human Protein Atlas (www.proteinatlas.org).

129 **Materials and Methods**

130 ***Ethics and tissue microarray design***

131 Human tissue samples from five tissue types were obtained from Uppsala University Hospital,
132 Sweden, and collected within the Uppsala Biobank organization. All samples were anonymized in
133 accordance with the approval and advisory report of the Uppsala Ethical Review Board (ref nos.
134 2002-577, 2005-388, 2007-159). The tissue microarray (TMA) was generated as previously
135 described[19] and comprised five distinct tissues: fallopian tube, endometrium, cervix, nasopharynx,
136 and bronchus (Figure 1B). Each tissue was represented by six one mm diameter cores, with
137 duplicate cores from three individuals. Patient information is provided in Supplementary Table 1.
138 The TMA was sectioned into 4 µm sections using a waterfall microtome (Microm H355S,
139 ThermoFisher Scientific, Fremont, CA) and mounted onto SuperFrost Plus slides (Thermo Fisher
140 Scientific, Fremont, CA). The slides were dried at room temperature (RT) overnight, baked at
141 50°C for 12–24 hours, cooled, and stored at RT until further use.

142

143 ***Multiplex panel development***

144 A fixed 5-plex panel was built to target five regions in ciliated cells: the cilium (CL), transition
145 zone (TZ), rootlet (RL), cytoplasm, and nucleus. Protein markers and corresponding antibodies
146 have been selected based on i) literature search (e.g. UniProtKB and scientific publications), ii)
147 antibody IHC reliability score on HPA[20] (see next section on Candidate selection), iii) expected
148 IHC staining patterns in ciliated cells in nasopharynx, bronchus, fallopian tube (FT), endometrium,
149 and cervix, and iv) compatibility with the multiplex immunohistochemistry (mIHC) panel and

150 workflow. Each antibody was first tested with a single-plex run, i.e. one antibody at a time, to
151 ensure that it worked equally well with the OPAL detection system, generating the same staining
152 pattern as with regular IHC. Then, each antibody was tested in each position of the mIHC workflow
153 to find the best location for each antibody to ensure a stable panel (Supplementary Table 2).
154 Finally, when the best position for each antibody was selected, all five panel markers were stained
155 simultaneously in a 5-plex staining, to confirm non-overlapping signals. To further validate the
156 three markers targeting the cilium structure, confocal microscopy at 63X was conducted using
157 Leica STELLARIS 5 (Leica Microsystems, Illinois, US).

158

159 ***Candidate selection***

160 Protein candidates and corresponding antibodies to be included in the present investigation were
161 selected based on publicly available data in the HPA, including scRNA-seq data, IHC antibody
162 reliability, and IHC staining pattern in human tissues. First, human scRNA-seq data from ciliated
163 cells was used. This cell type in the HPA Single Cell Type Resource[9] is based on external datasets
164 from bronchus, lung, endometrium and fallopian tube. The data is presented as normalized
165 transcripts per million (nTPM), showing the average expression of the cells in all cell type clusters
166 from these four tissue types that represent ciliated cells. In this study, genes showing an expression
167 level nTPM $\geq$ 0.1 were retained. Next, the IHC reliability score on HPA was considered, that
168 evaluates the expected staining pattern in the entire human body taking into consideration positive
169 and negative controls, literature, corresponding mRNA levels and similarity between multiple
170 antibodies targeting the same protein. This stringent antibody validation pipeline is divided into
171 four categories – Enhanced, Supported, Approved and Uncertain[20]. In this study, we restricted the

172 selection to only antibodies with Enhanced, Supported or Approved reliability score. From this
173 list, existing IHC annotation data from fallopian tube, bronchus and nasopharynx was considered,
174 consisting of proteins that previously have been identified to stain specific subsets of epithelial
175 cells in these tissues in the standard HPA pipeline. Finally, a manual curation was carried out based
176 on IHC staining patterns in all tissues with motile cilia that were included in the present
177 investigation, keeping only candidates with a distinct staining in ciliated cells, resulting in a refined
178 list of candidate markers (Figure 1A).

179

180 ***Slide pretreatment***

181 To remove paraffin and rehydrate tissue cores, a ST5010 Autostainer XL (Leica Biosystems,
182 Baden-Württemberg, Germany) was used with the following protocol: Xylene (5 min), Xylene (5
183 min), Xylene (1 min), absolute ethanol (3 min), absolute ethanol (3 min), 96% ethanol (3 min),
184 96% ethanol + 0.3% H_2O_2 (5 min), 80% ethanol (3 min), and dH_2O (30 sec). The slides were then
185 stored in deionized water until antigen retrieval.

186 Antigen retrieval was performed to expose protein epitopes for antibody binding. Slides were
187 subjected to heat-induced epitope retrieval (HIER) in pH 6 buffer (Agilent Technologies Inc.,
188 Santa Clara, CA, USA) at 125°C for 4 min using a Biocare Medical Decloaking Chamber™ PLUS
189 (DC2008INTL). After cooling to 90°C, the slides were rinsed in deionized water (1–2 min) and
190 transferred to TBS-Tween wash buffer (Thermo Fisher Scientific, TA-999-TT, Waltham, MA,
191 USA) until further processing. To reduce autofluorescence, slides were incubated in a bleaching
192 buffer containing 1.5% hydrogen peroxide, 0.2 M glycine, and 1X TBS-Tween (Thermo Fisher
193 Scientific, TA-999-TT) in 50-mL Falcon tubes. Tubes were rotated under an overhead LED light

194 at RT on a bench for 1 hour using a Stuart SRT9D roller mixer. Slides were subsequently washed
195 and stored in TBS-Tween until further use.

196

197 ***Multiplex immunofluorescence***

198 For multiplex immunofluorescence (mIF) staining, one slide per candidate protein was used. Each
199 of the six staining cycles proceeded as follows: Tissue sections were blocked with UV Blocking
200 Buffer (10 min) (UltraVision LP HRP kit, Epredia, Kalamazoo, MI), incubated with primary
201 antibody (30 min), rinsed in TBS-Tween, incubated with HRP-conjugated secondary antibody
202 (pre-conjugated ready-to-use) (10 min) (UltraVision LP HRP kit, Epredia), and washed again in
203 TBS-Tween. Slides were then incubated with the cycle-specific OPAL™ fluorophore (Akoya
204 Biosciences, Marlborough, MA) for 10 min, rinsed, and subjected to HIER (90°C, pH 6 buffer,
205 (Agilent Technologies Inc.) 20 min). The order of the Opal dyes and panel markers from first to
206 last cycle was: OPAL690 for CROCC, OPAL620 for DNAH9, OPAL520 for candidate protein
207 (changed for each slide), OPAL570 for AGR3, OPAL480 for NPHP4, and OPAL-DIG-780 for
208 FOXJ1. After each cycle, slides were rinsed and stored in wash buffer. The final step involved
209 incubating slides with OPAL 780 fluorophore-conjugated anti-DIG antibody (1:125 in Epredia™
210 Lab Vision™ Antibody Diluent OP Quanto, #TA-125-ADQ) for 1 hour, followed by staining with
211 DAPI (1:1000, Invitrogen, D1306, Thermo Fisher Scientific) for 5 min. Slides were rinsed,
212 mounted with Invitrogen ProLong™ Glass Antifade Mountant, covered, and cured overnight.
213 Finally, slides were digitized at 40X magnification using PhenoImager (Akoya Biosciences).

214

215 ***Image analysis***

216 A manual quality control was performed on all tissue cores, ensuring representativity of the
217 staining pattern, presence of ciliated cells and normal tissue histology. Tissue cores that did not
218 pass this quality control were not included in the data analysis. Automated image analysis was
219 conducted in ImageJ Fiji[21] to generate quantitative data. TIFF image stacks were processed per
220 TMA core (Supplementary Figure 1A). Each stack contained separate images for panel marker
221 proteins, DAPI, and autofluorescence. Images were converted to 8-bit, and DAPI/autofluorescence
222 images were discarded (Supplementary Figure 1B). Segmentation was performed using 3-level
223 Multi Otsu thresholding[22], where only the highest threshold level (brightest pixels) was used
224 (Supplementary Figure 1C). If segmentation failed for any marker, the stack was excluded from
225 further analysis. For each panel marker image, segmentation masks were generated
226 (Supplementary Figure 1D), defining regions of interest (ROIs) corresponding to each marker and
227 candidate protein (Supplementary Figure 1E). ROIs were used to extract pixel values from
228 candidate protein images by measuring the pixel value within each ROI, including mean pixel
229 intensity, maximum intensity, minimum intensity, and total ROI area per core.

230

231 ***Data analysis***

232 Data analysis was performed using R 4.4.2. Median intensity values were calculated per ROI (CL,
233 TZ, RL, cytoplasm, nucleus) for each protein and tissue, identifying predominant colocalization
234 patterns. Cores excluded during manual annotation were omitted from median calculations. Data
235 were normalized via Min-Max scaling per protein and slide across all tissues, with values rescaled
236 between 0 and 1. Heatmaps were generated based on image analysis results using the pheatmap

237 package (v1.0.12). Clusters in the heatmaps were generated using default Euclidean clustering
238 incorporated in the package. Gene Ontology (GO) enrichment analysis was conducted using
239 clusterProfiler (v4.14.6) and the human gene reference database org.Hs.eg.db (v3.20.0), retrieved
240 on 2025-02-25. Only GO terms with p.value < 0.05 were retained. The top three terms per cluster
241 were selected based on the highest number of associated proteins. The Protein Evidence (PE) and
242 Function Evidence (FE) scores for the candidate proteins were downloaded from the HPP portal[23]
243 on 2025/02/13.

244

245 **Results**

246 ***A high-throughput workflow to study subcellular location of proteins in ciliated cells***

247 Utilizing the extensive datasets in the publicly available HPA database (www.proteinatlas.org)[5],
248 we identified a total of 16,504 genes in the Single Cell Type resource that were expressed in the
249 ciliated cell cluster above the defined expression threshold. Among these, 10,197 proteins were
250 targeted by at least one antibody that met the IHC data reliability criteria, out of which 1,779
251 proteins were previously identified as having differential expression pattern in selected tissues
252 harboring motile ciliated cells. A final list of 187 candidates for further exploration was retained
253 following a manual examination of the IHC staining pattern in ciliated cells (Figure 1A;
254 Supplementary Table 3). A dedicated tissue microarray (TMA) was created, including five tissue
255 types known to harbor motile ciliated cells in both the respiratory and reproductive tracts:
256 nasopharynx (N), bronchus (B), fallopian tube (FT), endometrium (E), and cervix (C) (Figure 1B;
257 Supplementary Table 1). To precisely determine the localization of candidate proteins using an
258 iterative mIHC workflow, a fixed panel of five antibodies outlining different subcellular structures

259 of motile ciliated cells was developed (Figure 1C). The panel was combined with one antibody for
260 a new candidate protein to be studied per slide (Figure 1D). This design allowed for a standardized
261 high-throughput characterization of subcellular protein localization across multiple tissue samples.

262 The fixed panel was designed to map protein localization to five distinct subcellular regions of
263 ciliated cells defined by the cilium (CL), the transition zone (TZ), the rootlet (RL), the
264 cytoplasm, and the nucleus (Figure 2A). The final panel was based on the following proteins:
265 DNAH9 (Dynein Axonemal Heavy Chain 9), a component of the motile cilia axoneme, here
266 used as a marker for CL[24]; NPHP4 (Nephrocystin 4) localized in the TZ[25–27]; CROCC
267 (Rootletin), the main structural protein of the ciliary RL[28]; AGR3 (Anterior Gradient Protein 3),
268 described in mice as essential for regulating ciliary beat frequency, here used as a marker for
269 cytoplasm[29]; and the transcription factor FOXJ1 (Forkhead Box Protein J1), a key transcription
270 factor for motile cilia formation, an established marker for ciliated cell nucleus[11,30] (Figure 2B;
271 Supplementary Table 2). To validate the antibodies targeting the ciliary regions (CL, TZ, and
272 RL), we performed confocal microscopy at 63X magnification (Figure 2C). Given the complex
273 structure of the cilium, no substantial overlap was observed between these three markers,
274 reinforcing confidence in the panel. The final validated mIHC panel enabled the development of
275 image analysis pipelines and the definition of regions of interests (ROIs) based on the signals
276 obtained from each of the markers in the fixed panel, corresponding to the five distinct
277 subcellular localizations in ciliated cells (Supplementary Figure 1E).

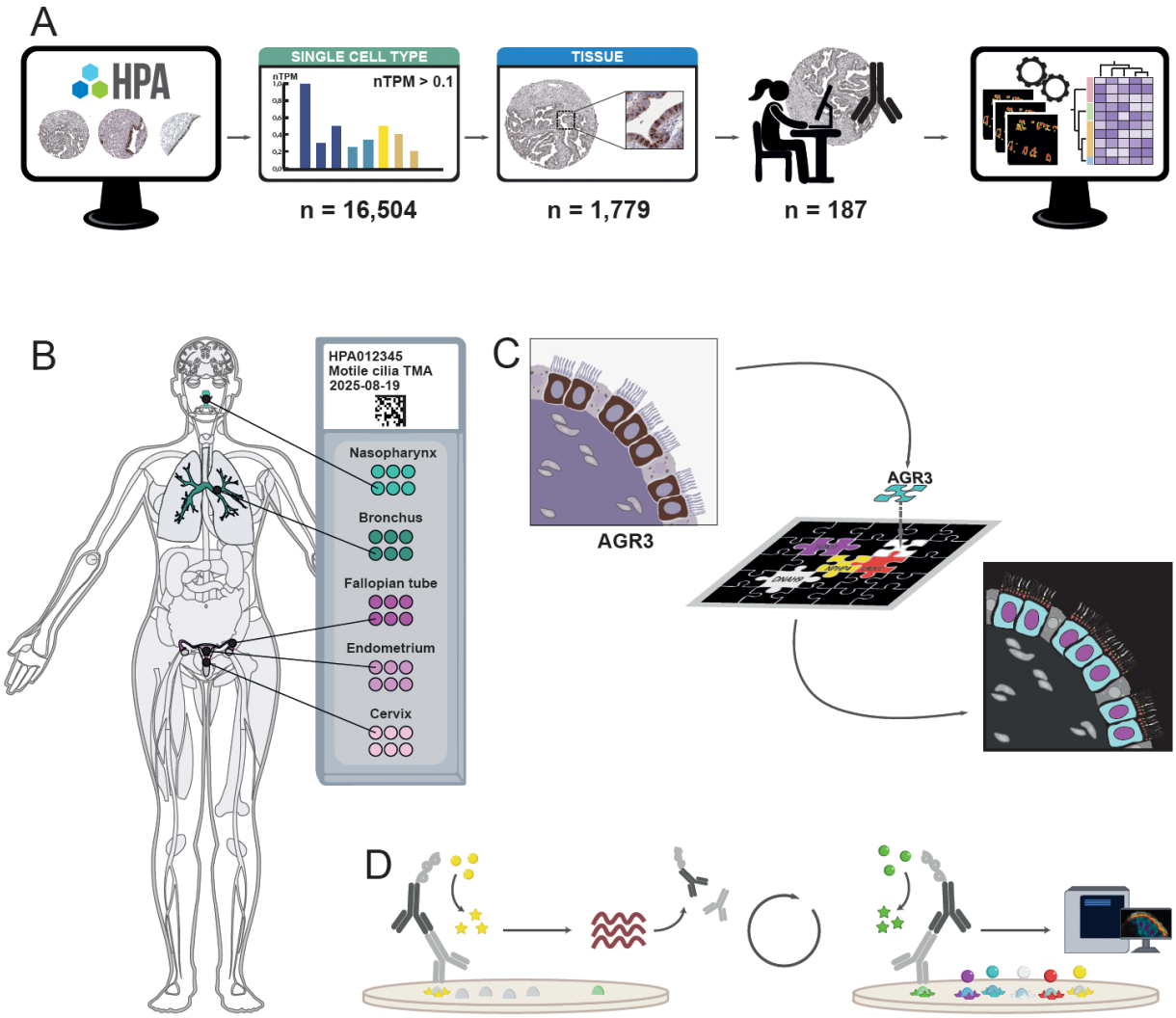

Figure 1: Experimental design. **A)** Selection of protein candidates from the Human Protein Atlas (www.proteinatlas.org) utilizing publicly available data from both the Single Cell Type and Tissue resources, allowing the identification of protein candidates expressed in ciliated cells with available reliably validated antibodies (n=187). The candidates were stained alongside the fixed antibody panel. Each acquired image was automatically analyzed to determine the expression profile, followed by clustering analysis. **B)** Five different tissues were collected and organized into a tissue microarray (TMA), consisting of two airway tissues (nasopharynx and bronchus) and three

287 reproductive tissues (fallopian tube, endometrium, cervix). For each tissue, six cores from three
288 patients were included. **C)** A multiplex immunohistochemistry (mIHC) antibody panel for ciliated
289 cells was developed based on a literature review and existing IHC data in the HPA Tissue resource,
290 here exemplified by the protein AGR3, showing staining in the cytoplasm of ciliated cells. The
291 antibodies targeted different subcellular compartments of ciliated cells: nucleus (magenta),
292 cytoplasm (cyan), rootlet (RL, red), transition zone (TZ, yellow), and cilium (CL, white). **D)**
293 Schematic representation of the mIHC workflow, with the first and last cycles illustrated. The
294 method relies on iterative cycles, each separated by heat-induced antibody stripping.

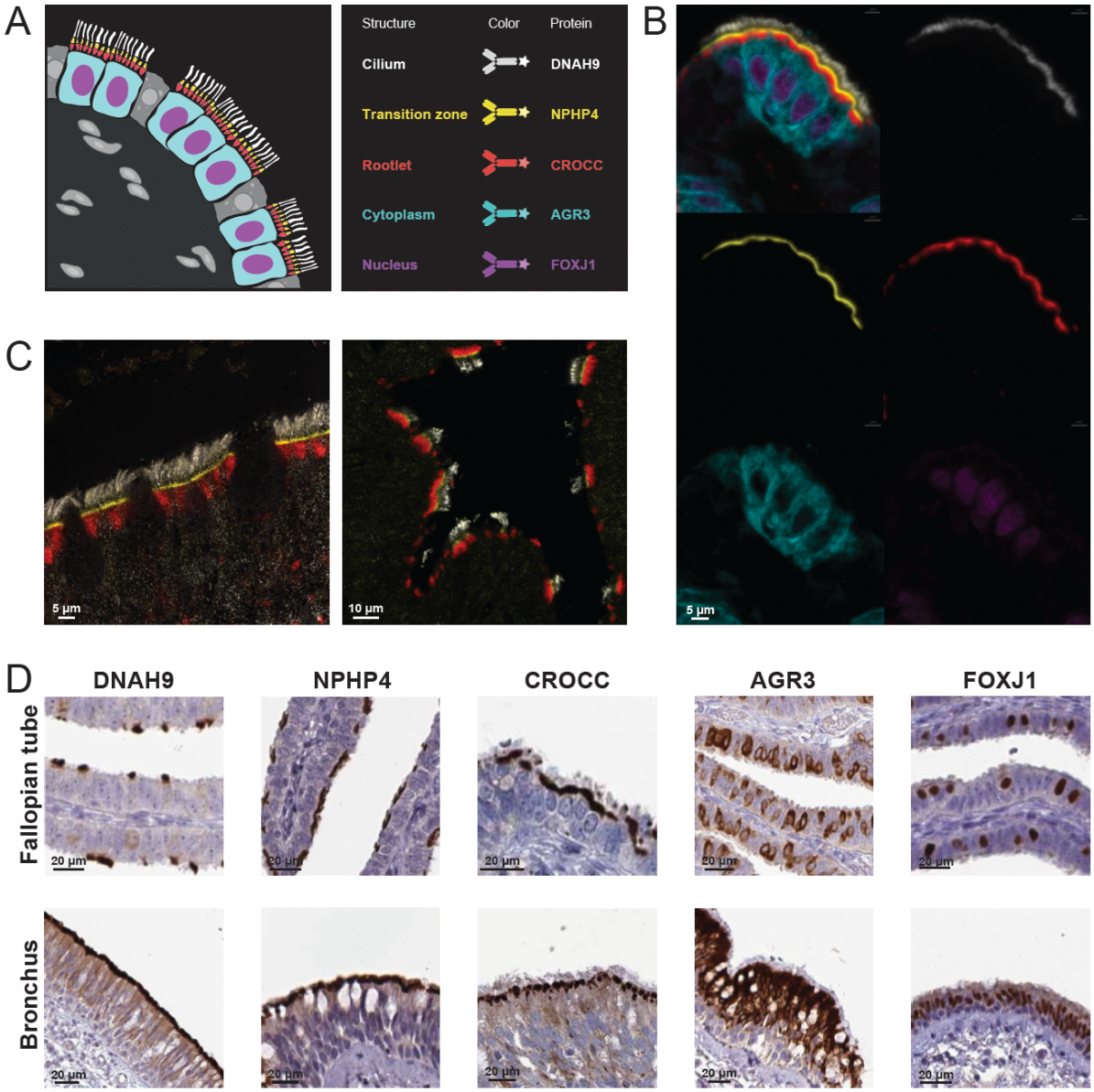

Figure 2: Validation and characterization of the fixed antibody panel. **A)** Schematic overview of the fixed panel used for mIHC stainings. The mIHC panel included five antibodies targeting proteins expressed in specific subcellular structures of ciliated cells: DNAH9 for the cilium (CL, white), NPHP4 for the transition zone (TZ, yellow), CROCC for the rootlet (RL, red), AGR3 for the cytoplasm (cyan), and FOXJ1 for the nucleus (magenta). **B)** Staining of the 5-plex fixed panel in ciliated cells of the fallopian tube. Top left: all five antibodies combined; top right: CL; middle

302 left: TZ; middle right: RL; bottom left: cytoplasm; bottom right: nucleus. **C)** Confocal microscopy
303 images. Confocal microscopy was used to validate the markers targeting ciliary structures. Non-
304 overlapping signals representing the CL (white), TZ (yellow), and RL (red) are shown in the
305 nasopharynx (left) and fallopian tube (right) at 63X resolution. **D)** IHC images from the HPA.
306 Antibodies included in the panel were selected based on literature, as well as their staining patterns
307 and reliability scores in the Tissue resource of the HPA.

308

309 ***Hierarchical clustering and functional annotation of ciliated cells proteins***

310 To address gaps in functional annotation, we integrated the FE scores defined by the HPP project[20]
311 with our 187 protein candidates (Supplementary Table 4) to assess the functional characterization
312 of the proteins included in our study. Interestingly, just over a quarter (27%, n=51) of the candidate
313 proteins stained alongside the panel fell into the FE1 category, indicating that at least one of their
314 functions has been described. However, the majority (73%, n=136) remain poorly or partially
315 characterized, with limited or no functional annotations (FE2 to FE5). To further examine the
316 relationship between protein function and clustering, we analyzed the distribution of FE scores
317 across clusters (Supplementary Figure 3). To provide a quantitative and systematic assessment of
318 expression levels, we developed an automated image analysis workflow to quantify pixel intensity
319 values for each analyzed protein and assess the subcellular localization of the staining patterns in
320 relation to the fixed antibody panel (Supplementary Figure 1). To determine the overlap between
321 each candidate protein and a specific area of the ciliated cells, the analysis method defined ROIs
322 based on each panel marker individually. Pixel intensity values within these ROIs were then
323 extracted from the images, allowing quantification of colocalization for each specific subcellular

structure (Supplementary Figure 1). To account for multiple images per protein per ROI and per tissue, a median pixel intensity value was calculated per protein and tissue type for each ROI, generating an expression profile across the tissues. The resulting quantitative protein expression levels were subsequently used for hierarchical clustering, which identified seven distinct protein clusters (Figure 3B). Clustering was also performed on ROI per tissue type, revealing that CL and TZ regions consistently grouped together across all tissues. In contrast, RL, cytoplasm, and nucleus displayed more heterogeneous localization patterns, with the cytoplasm and RL exhibiting the highest variability across tissues. Gene ontology (GO) enrichment analysis was performed for each cluster across the three GO categories: biological process (BP), molecular function (MF) and cellular component (CC). This analysis aimed to validate the expression patterns across different subcellular localizations and provide insights into the potential functions of the protein within each cluster (Figure 3C; Supplementary Table 5).

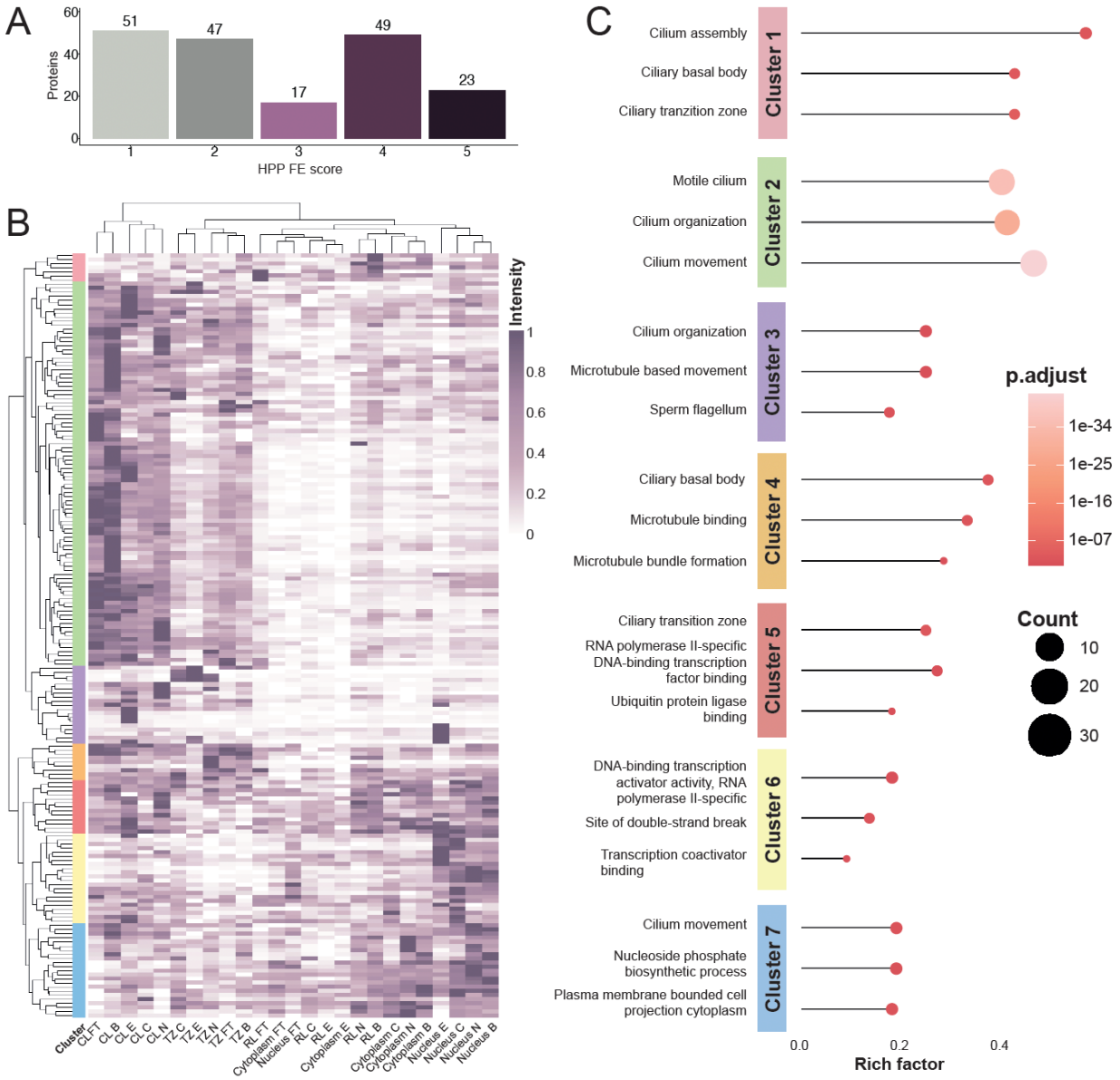

Figure 3: Functional evidence, Clustering Analysis, and Gene Ontology Enrichment. **A)** Bar plot showing the distribution of the studied protein between the different FE scores (FE1-5). **B)** A heatmap was generated based on expression levels obtained from image analysis for each candidate protein across different subcellular localizations and tissues (fallopian tube (FT), bronchus (B), endometrium (E), cervix (C), and nasopharynx (N). Hierarchical clustering was applied to both rows and columns. The columns were primarily clustered according to subcellular

344 localization rather than tissue type, particularly for ciliary structures such as the cilium (CL) and
345 transition zone (TZ). Row clustering identified seven distinct clusters based on the expression
346 patterns of the 187 candidate proteins. **B)** Bubble plot showing the top three Gene Ontology (GO)
347 terms of the three categories (BP, MF and CC) per cluster, with enrichment levels represented by
348 the rich factor i.e. the proportion of input genes annotated to a specific term relative to the total
349 genes associated with that term.

350

351 *Cluster 1: Basal body and ciliary core*

352 Cluster 1 (n = 7, primarily expressed in the RL, Figure 3B), was strongly linked to cilia, as
353 indicated by its top GO terms: cilium assembly, ciliary basal body, and ciliary transition zone
354 (Figure 3C). This suggests that proteins in this cluster play a central role in ciliary function. One
355 notable example is MDM2, which localized to the RL of the cilia in all five tissues and showed a
356 strong concordance between image observation and image analysis results (Figure 4A).
357 Interestingly, none of the 65 GO terms associated with MDM2 in our analysis; including response
358 to magnesium ion, cellular response to estrogen stimulus, positive regulation of intracellular
359 protein transport, and negative regulation of cell cycle G1/S phase transition; are directly related
360 to cilia or their structure. Although MDM2 is an FE1 protein with at least one well-characterized
361 function, its role in ciliated cells remains unclear.

362

363

364

365 *Cluster 2: Axonemal and motile cilia proteins*

366 Cluster 2 harbored the largest number of proteins (n = 94), with the top GO terms: motile cilium,
367 cilium organization, and cilium movement, indicating a strong association with motile cilia
368 specifically, rather than cilia in general (Figure 3C). The proteins in this cluster were primarily
369 detected in CL across all five analyzed tissues (Figure 3B). One example is NME9 (NME/NM23
370 family member 9, also known as TXNDC6 or TXL-2) (Figure 4B). While NME9 is highly
371 expressed in multiple tissues, with the highest mRNA level detected in the testis, previous studies
372 have shown that it localizes to airway epithelial cilia as a microtubule binding protein[31]. Here, we
373 demonstrated that NME9 is not restricted to the airway epithelium but is also present in the motile
374 cilia of three female reproductive tissues, where it exhibited similar staining intensity. Another
375 protein in Cluster 2 is LRRC73 (Leucine rich repeat containing 73) (Figure 4B). The mIHC
376 analysis indicated that LRRC73 was equally expressed in CL and RL but absent in TZ, with a
377 consistent pattern across all five tissues. However, no GO terms were identified for LRRC73 in
378 our analysis, nor are functional annotations available in UniProt, and it is ranked as a FE5 protein
379 (Supplementary Table 4 and 5). A third example is DPCD (Deleted in primary ciliary dyskinesia
380 homolog) (Figure 4B), a protein implicated in the function or formation of ciliated cells. Its highest
381 gene expression was observed in the testis, and previous studies have shown it is expressed in
382 sperm[32]. Our analysis confirmed that DPCD was specifically detected in CL of motile cilia in all
383 five tissues, with stronger expression in airway epithelial cilia compared to those in the female
384 reproductive tract. In humans, DPCD interacts with RUVBL1 and RUVBL2, proteins known to
385 be involved in dynein motor assembly, a crucial component for ciliary motility[33,34]. RUVBL1,
386 which fell into Cluster 7, was detected in the cytoplasm and nucleus of ciliated cells but not in the
387 ciliary structure (Figure 5C), in line with previous findings. GO terms identified for RUVBL1

388 include dynein axonemal particle, TFIID-class transcription factor complex binding, and ADP
389 binding (Supplementary Table 4). Notably, *Ruvbl1* knockdown in mice leads to axoneme structural
390 defects, further supporting its role as a ciliopathy-related protein essential for ciliary integrity[35].
391 Another protein found to be in Cluster 2 was ARMC2 (FE2), located in the cilium across all five
392 tissues (Supplementary Figure 4). It has been shown that PCD caused by *ARMC2* mutations not
393 only affects the reproductive system and abnormalities in sperm flagella[36], but also results in an
394 impaired airway system[37]. Here, spatial evidence is provided showing ARMC2 to be present in
395 motile cilia in both female reproductive and airway epithelium (Supplementary Figure 4). Our
396 analysis connected ARMC2 to multiple GO terms, such as cilium organization, cilium assembly,
397 and spermatid development. Finally, KIAA2012, a poorly characterized protein with no known
398 function (FE5) (Figure 4B; Supplementary Table 5) was also found in this cluster. Our data
399 revealed that it localized to CL of motile cilia across all five tissues, with similar expression levels
400 throughout, suggesting a conserved ciliary function.

401

402 *Cluster 3: Ciliary and flagellar motility proteins*

403 The top GO terms for Cluster 3 (n= 19), were cilium organization, microtubule-based movement,
404 and sperm flagellum (Figure 3C), highlighting its association with ciliary and flagellar structures.
405 One notable protein in this cluster is MS4A8 (Membrane spanning 4-domains A8, also known as
406 MS4A8b) (Figure 4C), a member of the MS4A protein family, that shares sequence and structural
407 homology with the IgE receptor CD20[38]. Here, we demonstrated that MS4A8 is specifically
408 localized to CL of motile ciliated cells across all five tissue types. MS4A8 has been ranked FE4
409 and interestingly also lacks previous evidence at the protein level (Supplementary Table 5). Our

410 findings here provide spatial evidence of MS4A8 protein expression, offering a valuable insight
411 into its potential role in motile cilia function.

412

413 *Cluster 4: Dual localization in axoneme and transition zone*

414 Cluster 4 (n = 9, with no FE1 proteins, Supplementary 3), presented a more complex expression
415 pattern, with overrepresentation in both CL and TZ (Figure 3B). The top GO terms identified were
416 ciliary basal body, microtubule binding, and microtubule bundle formation (Figure 3C),
417 highlighting the potential structural roles of these proteins in cilia. One key protein in this cluster
418 was SPAG6 (Sperm associated antigen 6) (Figure 4D), which is strongly linked to microtubule
419 bundle formation, cilium organization, and cilium movement (Supplementary Table 5). SPAG6 is
420 crucial for maintaining normal ciliary structure and function, and its loss has been associated with
421 brain edema in mice[39,40]. While SPAG6 deficiency leads to male infertility, female mice remain
422 fertile, although fertilization is delayed, suggesting an impact on the motile cilia in the oviduct[41].
423 In this study, SPAG6 showed widespread expression across the whole cell in bronchus and
424 nasopharynx, while its localization was more restricted to CL and TZ in endometrium and cervix
425 (Figure 4D). Another protein in this cluster is LRRC45 (Leucine rich repeat containing 45), which
426 was primarily localized to CL, as well as TZ and RL (Figure 4D). Previously described in primary
427 cilia, defects of LRRC45 are thought to alter ciliary length and beat frequency[42,43]. Here, we
428 showed its presence and specific localization in motile cilia across both the respiratory and
429 reproductive tract. However, our GO term analysis did not identify any functional annotation for
430 LRRC45, and it is classified as FE5 (Supplementary Table 5), indicating that its precise role
431 remains to be elucidated.

432 *Cluster 5: Ciliated proteins with diverse localization*

433 In Cluster 5 (n = 13), protein expression patterns were distributed across the entire ciliated cell
434 (Figure 3B). The GO terms identified in this cluster were ciliary transition zone, RNA polymerase
435 II-specific DNA-binding transcription factor binding, and Ubiquitin protein ligase binding,
436 suggesting a broad functional involvement in cellular activity (Figure 3C). One example is RIIAD1
437 (Regulatory subunit of type II PKA R-subunit domain containing 1), which was predominantly
438 localized in CL, TZ, cytoplasm and nucleus across all examined tissues (Figure 5A). Although
439 RIIAD1 remains poorly characterized, studies have reported its upregulation in breast cancer
440 tumors[44,45]. Notably, our GO term analysis did not identify any functional annotations for this
441 protein, which is classified as a FE5 protein (Supplementary Table 4), suggesting its role in motile
442 cilia should be examined. Another protein in this cluster is SGMS2 (Sphingomyelin synthase 2),
443 which was detected in all targeted locations in the ciliated cells across all tissues, although
444 significantly lower presence was observed in RL in the reproductive tissues (Figure 5A). SGMS2
445 is classified as a FE1 protein (Supplementary Table 4), indicating strong evidence for a molecular
446 function. While our GO term analysis identified phosphotransferase activity for other substituted
447 phosphate groups as a related term (Supplementary Table 5), additional annotations, including
448 nucleoplasm, plasma membrane, and sphingomyelin synthase activity, suggest broader functional
449 roles.

450

451

452

453 *Cluster 6: Nuclear and cytoplasmic proteins*

454 Cluster 6 (n = 22) consisted of proteins primarily localized to the cytoplasm and nucleus (Figure
455 3B), as supported by the top three GO terms: DNA-binding transcription activator activity, RNA
456 polymerase II-specific, site of double-strand break, and transcription coactivator binding (Figure
457 3C). Notably, 45% of the proteins (n=10) in this cluster are classified as FE1, indicating strong
458 evidence of the molecular function (Supplementary Figure 3). One key protein of this cluster is
459 WRAP53 (WD repeat containing antisense to TP53) (Figure 5B), classified as FE1
460 (Supplementary Table 4). The GO term enrichment identified the site of double-strand break as a
461 related function (Supplementary Table 5), aligning with its known role in DNA damage response.
462 WRAP53 is recruited to the site of a double strand break (DSB), where it facilitates the recruitment
463 of other DNA repair proteins[46]. Here, we showed that WRAP53 was predominantly expressed in
464 the nucleus of ciliated cells across all tissues. Another protein in this cluster is SAMHD1 (SAM
465 and HD domain containing deoxynucleoside triphosphate triphosphohydrolase 1) (Figure 5B), also
466 classified as FE1 (Supplementary Table 4). Like WRAP53, SAMHD1 is associated with the GO
467 term site of double-strand break (Supplementary Table 4). We revealed its nuclear localization in
468 ciliated cells across all five tissues, reinforcing its potential role in DNA repair mechanisms.
469

470 *Cluster 7: mixed localization with ciliary and cytoplasmic functions*

471 The final cluster, Cluster 7 (n = 23), exhibited less specific localization patterns compared to other
472 clusters, with proteins predominantly found in the cytoplasm and the nucleus (Figure 3B). GO
473 term analysis identified key biological functions, including cilium movement, nucleoside
474 phosphate biosynthetic process, and plasma membrane bounded cell projection cytoplasm (Figure

475 3C). Among the proteins in this cluster, RUVBL1 was previously mentioned with proteins from
476 cluster 2 (Figure 5C) and classified as FE1 (Supplementary Table 4). Another protein in this cluster
477 is CFAP73 (Cilia and flagella associated protein 73), classified as FE4 (Supplementary Table 4),
478 which was primarily expressed in the cytoplasm and, to a lesser extent, in the nucleus across all
479 tissues (Figure 5C). GO analysis linked CFAP73 to essential ciliary processes, including cilium
480 movement, axonemal dynein complex assembly, and cilium organization (Supplementary Table
481 5), suggesting a role in ciliary structure and function.

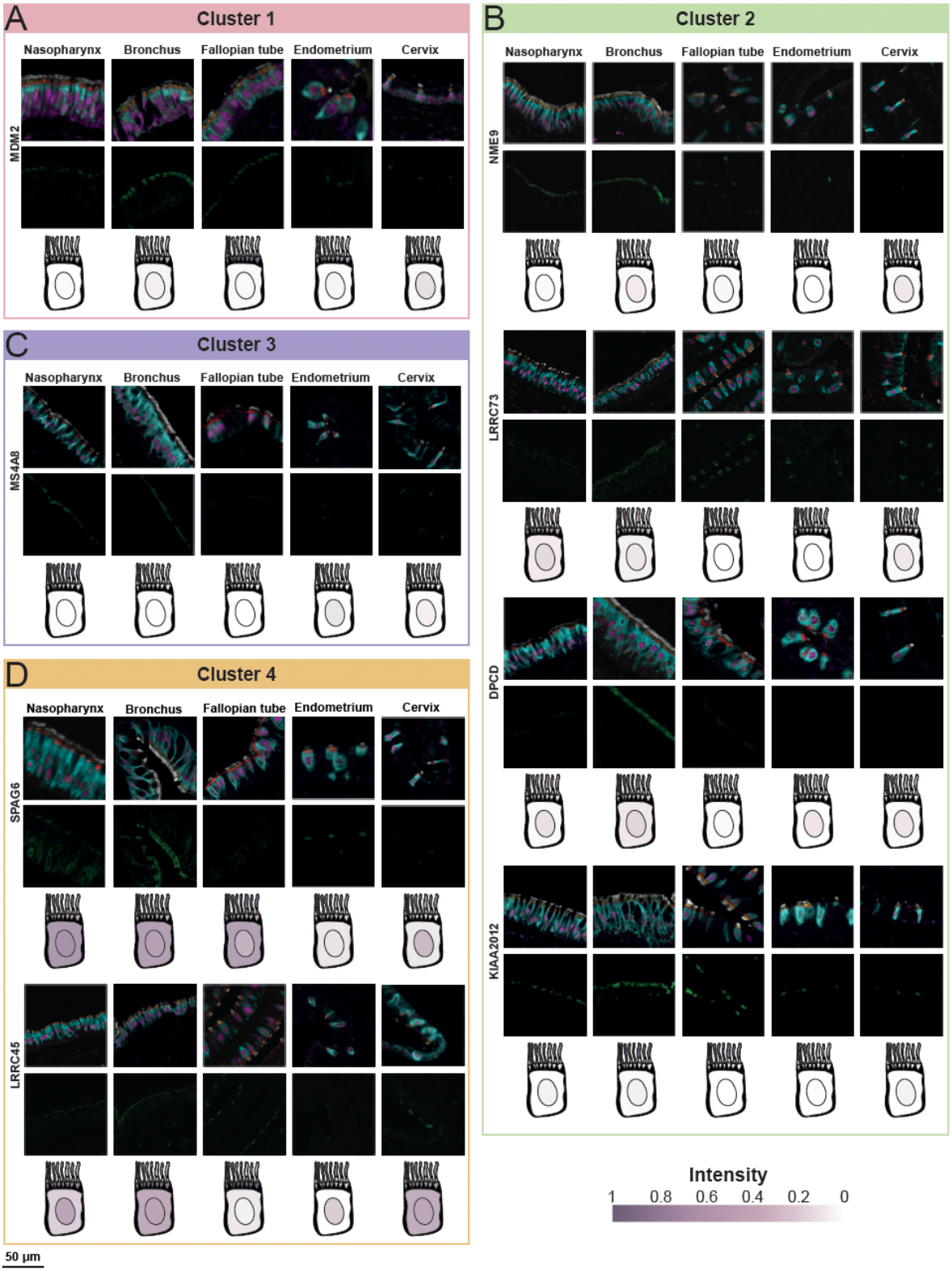
A
Cluster 1
Nasopharynx
Bronchus
Fallopian tube
Endometrium
Cervix
MDM2
B
Cluster 2
NME9
LRRC73
DPCD
KIAA2012
C
Cluster 3
MS4A8
D
Cluster 4
SPAG6
LRRC45
Intensity
1 0.8 0.6 0.4 0.2 0
50 µm

482

483 ***Figure 4: mIHC staining of representative proteins from each cluster across different tissues***.
484 The top row of images shows the composite staining, including the fixed panel and the candidate
485 protein. The bottom row displays only the candidate protein (in green). Below the images, a
486 schematic representation of a ciliated cell illustrates the expression levels obtained from image
487 analysis for each subcellular localization. A) Cluster 1: MDM2 (RL) B) Cluster 2: NME9 (CL),
488 LRRC73 (CL and RL), DPCD (CL), and KIAA2012 (CL). C) Cluster 3: MS4A8 (CL). D) Cluster
489 4: SPAG6 (whole cell in bronchus and nasopharynx; CL and TZ in endometrium and cervix) and
490 LRRC45 (CL, TZ and RL).

491

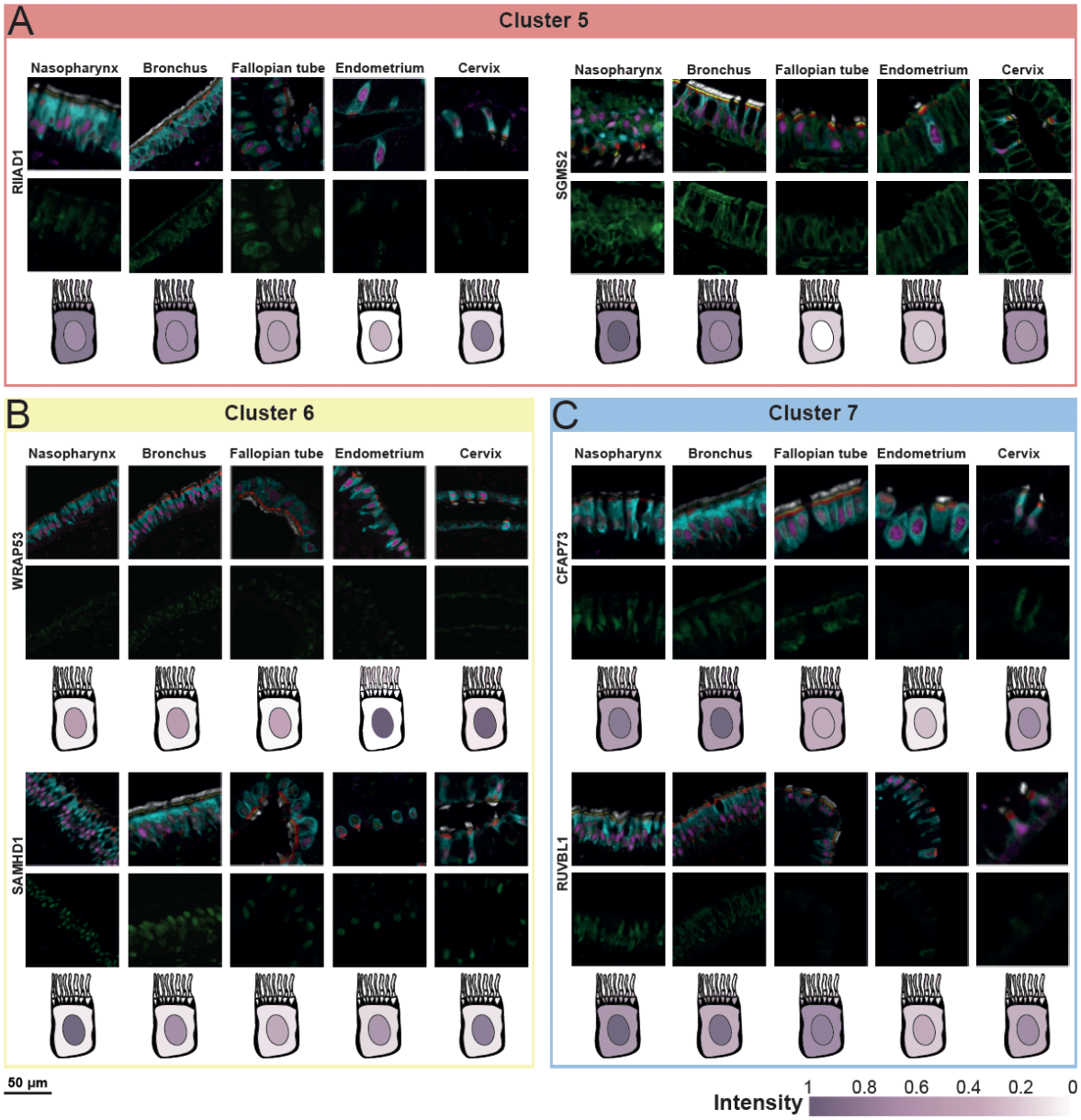

492

493 ***Figure 5: mIHC staining of representative proteins from each cluster across different tissues.***
494 The top row of images shows the composite staining, including the fixed panel and the candidate
495 protein. The bottom row displays only the candidate protein (in green). Below the images, a
496 schematic representation of a ciliated cell illustrates the expression levels obtained from image
497 analysis, the darker the color, the higher the expression level. **A**) Cluster 5: RIIAD1 (CL, TZ,

498 cytoplasm and nucleus) and SGMS2 (whole cell). **B**) Cluster 6: WRAP53 (nucleus) and SAMHD1
499 (nucleus). **C**) Cluster 7: CFAP73 (cytoplasm and nucleus) and RUBBL1 (cytoplasm and nucleus).

500

501 **Discussion**

502 This study introduces a comprehensive mIHC and automated image analysis workflow designed
503 to investigate the subcellular localization of proteins in motile ciliated cells at a high resolution.
504 To our knowledge, this is the first approach to combine high-resolution tissue imaging of motile
505 ciliated cells with the scalability of high-throughput analysis of a large set of proteins across
506 multiple tissue types using an in-house medium-plex panel tailored for this purpose. The unique
507 panel and novel workflow were successfully used to spatially map 187 proteins in ciliated cells
508 across five human tissues from both respiratory and female reproductive tracts. Protein localization
509 was determined based on the overlap with a fixed reference panel outlining distinct subcellular
510 compartments of motile ciliated cells. The validated panel enabled precise localization and
511 quantification of each of the candidate proteins within five defined subcellular regions: the
512 nucleus, cytoplasm, and three cilia-specific compartments: CL, TZ, and RL[17].

513 The 187 candidate proteins studied in the present investigation were selected using two key
514 resources of the Human Protein Atlas (HPA): i) the Single Cell Type resource, to validate the
515 transcript-level expression in ciliated cells compared to other cell types in the studied tissues, and
516 ii) the Tissue resource, to prioritize candidates with reliable antibodies showing positive IHC
517 staining in ciliated cells in at least one of the five analyzed tissues included in the study. Using the
518 cut-off threshold of 0.1 nTPM enabled the inclusion of a broad spectrum of proteins, encompassing
519 both cilia specific markers and proteins with more ubiquitous expression profiles across different

520 cell types (Supplementary Figure 2). As some proteins are broadly expressed across multiple cell
521 types, immunostaining outside the ciliated cells population was occasionally observed and could
522 be detected upon manual examination. The image analysis pipeline was however restricted to the
523 predefined panel markers specifically targeting ciliated cells, and as a result quantitative data on
524 protein expression in other cell types was not generated as part of this effort. One example of such
525 a protein is GALNS (images not shown), that in addition to staining in ciliated cells also showed
526 positivity in other epithelial cells and immune cells. Even if some proteins are not specific to
527 ciliated cells from a body-wide perspective, we still believe that a detailed mapping of these
528 proteins in ciliated cells aids in understanding their potential role in cilia function.

529 While most of the proteins encoded by the human genome have been credibly identified, many
530 proteins still lack a specifically defined function based on experimental evidence. One of the major
531 goals of the international consortium HPP is to gain a solid understanding of at least one function
532 for every protein at the molecular level[47]. As a result, the HPP has introduced the definition of
533 Function Evidence (FE) scores that build upon the functional information available in the
534 UniProtKB, described as FE1-FE5 according to the level of evidence for a molecular function[47].
535 These new FE scores have been implemented for each protein encoded by the human genome.
536 Interestingly, a majority (73%) of the candidate proteins characterized in our study showed FE2-
537 FE5 scores, indicating that a full understanding of the role of these proteins in ciliated cells is still
538 lacking. Our stringent validation pipeline and detailed data presenting a specific localization to
539 ciliated cells at a subcellular resolution gives further insights into a presumed function of these
540 proteins. The spatial localization data constitutes a starting point for further functional studies
541 using e.g. model systems, to determine the roles of these proteins in each of the analyzed tissue
542 types.

543 For further functional analysis, we also performed a hierarchical clustering analysis of the
544 candidate proteins for each of the analyzed tissues using quantitative protein localization data
545 generated by automated image analysis. The clustering analysis revealed that protein localization
546 was largely conserved across tissues, particularly for CL and TZ, suggesting a shared spatial
547 distribution for these proteins. Similarly, candidate proteins clustered based on their expression
548 patterns, resulting in seven distinct expression groups. While some clusters exhibited clear
549 localization patterns, such as cluster 2, with proteins mainly expressed in the cilium, or cluster 6,
550 in the nucleus; others, like cluster 5, displayed a more dispersed expression profile. Nevertheless,
551 the clustering analysis allowed us to group the proteins according to expression patterns,
552 highlighting numerous poorly described proteins that shared a similar expression profile with well-
553 described cilia markers, thus indicating a similar molecular function. We also performed a GO
554 analysis for each of the expression clusters, which revealed a clear overrepresentation of cilia-
555 associated functions, thus validating our strategy and providing an initial framework for a deeper
556 understanding of protein function. It should however be noted that proteins localized to general
557 cellular compartments such as the cytoplasm or nucleus may still exhibit cilia-specific roles. Given
558 that GO annotations are derived from data across multiple cell types or model systems and not
559 exclusively motile ciliated cells in the *in situ* context described here, definitive conclusions
560 regarding specific functional or biological processes require further targeted investigation.

561 To confirm the validity of our approach, the list of candidates included several well-characterized
562 proteins belonging to families with known functions in cilia, (such as cilia and flagella associated
563 proteins (CFAPs), coiled-coil domain-containing proteins (CCDCs), dynein axonemal heavy chain
564 proteins (DNAHs) and dynein axonemal intermediate chain proteins (DNAIs). We also shed light
565 on several proteins with only limited evidence, such as seven different open reading frame proteins

566 (C15orf48, C1orf87, C20orf8, C2orf50, C4orf47, C6orf132 and C7orf57) and other proteins with
567 no previous description in the context of cilia biology, e.g. KIAA2012, RIIAD1 and MS4A8. Here
568 we show for the first time that these proteins are expressed in specific subcellular compartments
569 of motile ciliated cells. KIAA2012, a poorly described protein located in the cilium compartment
570 (CL region) of motile ciliated cells in both respiratory and female reproductive tissues. Based on
571 its subcellular location, it can be anticipated that this protein may contribute to cilia motility and
572 thereby has the potential to cause primary ciliary dyskinesia (PCD) where the function of motile
573 cilia is impaired, a syndrome causing a wide range of symptoms and diseases[12]. Another protein
574 with limited characterization is RIIAD1, previously shown to be upregulated in breast cancer
575 tumors, but without a known molecular function. The name of the protein suggests that it regulates
576 a subunit of protein kinase A (PKA), involved in endocrine signaling and previously described to
577 play a crucial role in regulating ciliary beating frequency[48]. Here, we show that this protein is
578 generally expressed across the whole ciliated cell, both in the cell body and the cilium, in all five
579 analyzed tissues. Interestingly, scRNA levels in other analyzed tissues in the Single Cell Type
580 resource of the HPA show that expression is dominated in ciliated cells, followed by early
581 spermatids, and cone photoreceptor cells. As mature sperm contain flagella, with a similar
582 molecular function related to motility as ciliated cells[49], and photoreceptor cells contain specialized
583 sensory cilia[50], the mRNA expression levels together with the spatial localization pattern suggests
584 that this protein may be crucial for regulating and supporting key ciliary functions. Our study
585 included numerous other proteins that lack a description of molecular function or were not
586 previously described in the context of cilia biology, including MS4A8 which previously only has
587 been described at the transcript level. Here, we could provide the first spatial evidence that this
588 protein is expressed in the cilium of motile ciliated cells.

589 The selection of proteins included in the present investigation was mostly focusing on conserved
590 motile ciliary proteins present in all the analyzed tissues, but we did identify several proteins whose
591 expression pattern differed between respiratory and reproductive tissues. This shows that our
592 workflow has the potential of cross-tissue comparison and that motile cilia may have different
593 proteomes in different human tissue compartments, a finding that may explain phenotypic diversity
594 in motile ciliopathy patients. Further studies using our novel strategy for mapping the entire motile
595 cilia proteome in health and disease are expected to give unprecedented insights into the field of
596 cilia biology.

597 Importantly, our method is facing limitations in resolution: Proteins detected in the TZ region
598 might not necessarily be part of the TZ but localize close to it, at the rootlet or at the proximal
599 cilium. Similarly, proteins that we discover in the CL region might not localize in the axoneme but
600 in the cilioplasm or ciliary membrane. And we may detect proteins in the RL region that belong
601 either to the RL or to broader structures close to the RL or in the basal body (BB). Nevertheless,
602 our workflow provides a resolution not attainable by regular IHC, and a starting point for
603 identifying subcellular expression patterns of ciliary proteins that can be validated by other
604 molecular approaches.

605 In the rapidly expanding field of spatial biology, a multitude of methods focus on multiplexed
606 imaging of proteins. Here, we developed a novel “medium-plex” workflow, centered around a
607 fixed antibody panel outlining five different subcellular compartments of motile ciliated cells.
608 While higher-plex methods enable the simultaneous analysis of multiple cell types and structures
609 within a given tissue, our approach offers the advantage of subcellular-level resolution combined
610 with high-throughput capacity, making it well suited for both proteome-wide investigation and
611 clinical routine. This strategy provides a powerful foundation for comprehensive mapping of the

612 motile cilia proteome in both health and disease. It represents an important step toward uncovering
613 the molecular mechanisms driving ciliopathy and paves the way for future applications in precision
614 diagnostics and personalized medicine.

615

616

617 ASSOCIATED CONTENT

618 The following files are available free of charge (separate file (s)).

619 **Supplementary Figure 1:** Image analysis workflow

620 **Supplementary Figure 2:** mRNA expression levels across different cell types based on scRNA
621 sequencing data for the 187 candidates included in the study

622 **Supplementary Figure 3.** Bar plot showing the distribution of FE scores across each expression
623 **cluster.**

624 **Supplementary Figure 4.** mIHC staining of ARMC2 in the cilium in different tissues.

625 **Supplementary Table 1:** Patient information for all tissue samples included in the TMA

626 **Supplementary Table 2:** Information for the antibodies included in the fixed panel

627 **Other Supplementary Materials for this manuscript include the following:**

628 **Supplementary Table 3:** Information about the antibodies used to map the 187 protein candidates
629 included in the study (separate .xlsx file)

630 **Supplementary Table 4:** Protein Evidence (PE) and Function Evidence (FE) scores from the HPP
631 for the 187 candidate proteins included in the study (separate .xlsx file)

632 **Supplementary Table 5:** Protein expression levels based on automated image analysis, and results
633 based on gene ontology enrichment for the 187 protein candidates included in the study (separate
634 .xlsx file)

635

636 AUTHOR INFORMATION

637 Corresponding author:
638 Cecilia Lindskog
639 Department of Immunology, Genetics and Pathology
640 Cancer Precision Medicine Research Unit
641 Uppsala University, SE-75185 Uppsala, Sweden
642 Tel: +46 18 471 50 32
643 Email: cecilia.lindskog@igp.uu.se

644 Author Contributions

645 Conceptualization: CL and LM; Data curation: FB and LM; Formal Analysis: FB and LM;
646 Funding acquisition: CL and MU; Investigation: FH, LM, JNH, FB; Methodology: CL, FB, LM
647 and FH; Project administration: CL and LM; Resources: CL and LM; Image analysis: FB, FH,
648 LM; Supervision: CL, LM, FH; Validation: FB, LM, and CL; Visualization: FB and LM;

Writing – original draft: FB, LM and CL; Writing – review & editing: FB, LM, CL, FH, JNH and MU. All authors have read and approved the final version of the manuscript.

Funding Sources

CL: Swedish Research Council (2022–02742)

MU: Knut and Alice Wallenberg Foundation (2015.0344)

JNH: Postdoctoral Fellowship from the Wenner-Gren Foundations and EMBO Postdoctoral Fellowship (ALTF 556-2022)

Notes

Competing interests: Authors declare that they have no competing interests.

Data availability

Out of the 187 proteins, 175 were made available in HPA version 25 (v25.proteinatlas.org). The remaining will be available in a repository up on publication.

Code availability

The script for image analysis (Macros) and data analysis (R) used for data analysis and visualization is available on GitHub:

github.com/LindskogLab/Subcellular-map-of-proteins-in-ciliated-cells

670 ACKNOWLEDGMENT

671 We thank the Biological Visualization platform BioVis at Uppsala university for their vast help in
672 imaging and image analysis. We also thank the patients who donated tissues for HPA. Lastly, we
673 thank the members of HPA supporting this project in any way, especially Jonas Gustavsson,
674 Rutger Schutten, and Borbala Katona.

675

676 ABBREVIATIONS

677 AI - artificial intelligence; B – bronchus; BB – basal body; BP - biological process; C - cervix; CC
678 - cellular component; CL - cilium; DSB - double-strand break; E - endometrium; FE - function
679 evidence; FT - fallopian tube; GO - gene ontology; HIER - heat-induced epitope retrieval; HPA -
680 Human Protein Atlas; HPP - Human Proteome Project; HRP - horseradish peroxidase; IgE –
681 immunoglobulin E; IHC - immunohistochemistry; MF - molecular function; mIHC - multiplex
682 immunohistochemistry; N - nasopharynx; PCD - primary ciliary dyskinesia; PE - protein evidence;
683 PKA – protein kinase A; QC - quality control; RL - rootlet; ROI - regions of interest; RT - room
684 temperature; scRNA - single-cell RNA; TMA - tissue microarray; TZ - transition zone

685

686

687

688 REFERENCES

689 1. Hung, M.-C. & Link, W. Protein localization in disease and therapy. *Journal of Cell Science*
690 **124**, 3381–3392 (2011).

691 2. Thul, P. J. *et al.* A subcellular map of the human proteome. *Science* **356**, eaal3321 (2017).

692 3. Adhikari, S. *et al.* A high-stringency blueprint of the human proteome. *Nat Commun* **11**, 5301
693 (2020).
694 4. Omenn, G. S. *et al.* The 2024 Report on the Human Proteome from the HUPO Human
695 Proteome Project. *J Proteome Res* **23**, 5296–5311 (2024).
696 5. Uhlén, M. *et al.* Tissue-based map of the human proteome. *Science* **347**, 1260419 (2015).
697 6. Method of the Year 2024: spatial proteomics. *Nat Methods* **21**, 2195–2196 (2024).
698 7. Ghoshal, B., Hikmet, F., Pineau, C., Tucker, A. & Lindskog, C. DeepHistoClass: A Novel
699 Strategy for Confident Classification of Immunohistochemistry Images Using Deep Learning.
700 *Mol Cell Proteomics* **20**, 100140 (2021).
701 8. Shariff, A., Kangas, J., Coelho, L. P., Quinn, S. & Murphy, R. F. Automated Image Analysis
702 for High-Content Screening and Analysis. *J Biomol Screen* **15**, 726–734 (2010).
703 9. Karlsson, M. *et al.* A single–cell type transcriptomics map of human tissues. *Sci Adv* **7**,
704 eabh2169 (2021).
705 10. Reiter, J. F. & Leroux, M. R. Genes and molecular pathways underpinning ciliopathies. *Nat*
706 *Rev Mol Cell Biol* **18**, 533–547 (2017).
707 11. Pedersen, L. B., Jurisch-Yaksi, N., Schmid, F. & Christensen, S. T. Cilia and Flagella. in
708 *Encyclopedia of Cell Biology (Second Edition)* (eds Bradshaw, R. A., Hart, G. W. & Stahl, P.
709 D.) 164–188 (Academic Press, Oxford, 2023). doi:10.1016/B978-0-12-821618-7.00209-1.
710 12. Wallmeier, J. *et al.* Motile ciliopathies. *Nat Rev Dis Primers* **6**, 1–29 (2020).
711 13. Narayan, D. *et al.* Unusual inheritance of primary ciliary dyskinesia (Kartagener's syndrome).
712 *J Med Genet* **31**, 493–496 (1994).
713 14. Krawczyński, M. R., Dmeńska, H. & Witt, M. Apparent X-linked primary ciliary dyskinesia
714 associated with retinitis pigmentosa and a hearing loss. *J Appl Genet* **45**, 107–110 (2004).

715 15. Despotes, K. A., Zariwala, M. A., Davis, S. D. & Ferkol, T. W. Primary Ciliary Dyskinesia:
716 A Clinical Review. *Cells* **13**, 974 (2024).
717 16. Fliegauf, M., Benzing, T. & Omran, H. When cilia go bad: cilia defects and ciliopathies. *Nat*
718 *Rev Mol Cell Biol* **8**, 880–893 (2007).
719 17. Ishikawa, T. Structure of Motile Cilia. in *Macromolecular Protein Complexes IV: Structure*
720 *and Function* (eds Harris, J. R. & Marles-Wright, J.) 471–494 (Springer International
721 Publishing, Cham, 2022). doi:10.1007/978-3-031-00793-4_15.
722 18. Gopalakrishnan, J. *et al.* Emerging principles of primary cilia dynamics in controlling tissue
723 organization and function. *EMBO J* **42**, e113891 (2023).
724 19. Kampf, C., Olsson, I., Ryberg, U., Sjöstedt, E. & Pontén, F. Production of Tissue Microarrays,
725 Immunohistochemistry Staining and Digitalization Within the Human Protein Atlas. *J Vis Exp*
726 3620 (2012) doi:10.3791/3620.
727 20. Sivertsson, Å. *et al.* Enhanced Validation of Antibodies Enables the Discovery of Missing
728 Proteins. *J Proteome Res* **19**, 4766–4781 (2020).
729 21. Schindelin, J. *et al.* Fiji: an open-source platform for biological-image analysis. *Nat Methods*
730 **9**, 676–682 (2012).
731 22. 廖炳松, 陳澤生 & 詹寶珠. A Fast Algorithm for Multilevel Thresholding. *Journal of*
732 *Information Science and Engineering* **17**, 713–727 (2001).
733 23. HPP Portal. https://hppportal.net/.
734 24. Fliegauf, M. *et al.* Mislocalization of DNAH5 and DNAH9 in Respiratory Cells from Patients
735 with Primary Ciliary Dyskinesia. *Am J Respir Crit Care Med* **171**, 1343–1349 (2005).
736 25. Awata, J. *et al.* NPHP4 controls ciliary trafficking of membrane proteins and large soluble
737 proteins at the transition zone. *J Cell Sci* **127**, 4714–4727 (2014).

738 26. Fliegauf, M. *et al.* Nephrocystin Specifically Localizes to the Transition Zone of Renal and
739 Respiratory Cilia and Photoreceptor Connecting Cilia. *Journal of the American Society of*
740 *Nephrology* **17**, 2424 (2006).
741 27. Czarnecki, P. G. & Shah, J. V. The ciliary transition zone: From Morphology and Molecules
742 to Medicine. *Trends Cell Biol* **22**, 201–210 (2012).
743 28. Nechipurenko, I. V. *et al.* A conserved role for Girdin in basal body positioning and
744 ciliogenesis. *Dev Cell* **38**, 493–506 (2016).
745 29. Bonser, L. R. *et al.* The Endoplasmic Reticulum Resident Protein AGR3. Required for
746 Regulation of Ciliary Beat Frequency in the Airway. *Am J Respir Cell Mol Biol* **53**, 536–543
747 (2015).
748 30. Wallmeier, J. *et al.* De Novo Mutations in FOXJ1 Result in a Motile Ciliopathy with
749 Hydrocephalus and Randomization of Left/Right Body Asymmetry. *Am J Hum Genet* **105**,
750 1030–1039 (2019).
751 31. Sadek, C. M. *et al.* Characterization of Human Thioredoxin-like 2. *J Biol Chem* **278**, 13133–
752 13142 (2003).
753 32. Zariwala, M. *et al.* Investigation of the Possible Role of a Novel Gene, DPCD, in Primary
754 Ciliary Dyskinesia. *Am J Respir Cell Mol Biol* **30**, 428–434 (2004).
755 33. Liu, G., Wang, L. & Pan, J. Chlamydomonas WDR92 in association with R2TP-like complex
756 and multiple DNAAFs to regulate ciliary dynein preassembly. *J Mol Cell Biol* **11**, 770–780
757 (2018).
758 34. Li, Y. *et al.* Cotranslational molecular condensation of cochaperones and assembly factors
759 facilitates axonemal dynein biogenesis. *Proc Natl Acad Sci U S A* **121**, e2402818121.

760 35. Dafinger, C. *et al.* Targeted deletion of the AAA-ATPase Ruvbl1 in mice disrupts ciliary
761 integrity and causes renal disease and hydrocephalus. *Exp Mol Med* **50**, 1–17 (2018).
762 36. Coutton, C. *et al.* Bi-allelic Mutations in ARMC2 Lead to Severe Astheno-Teratozoospermia
763 Due to Sperm Flagellum Malformations in Humans and Mice. *Am J Hum Genet* **104**, 331–340
764 (2019).
765 37. Wu, B. *et al.* Broadening the ARMC2 mutational phenotype: linking multiple morphological
766 abnormalities of the Flagella to Pulmonary Manifestations in Primary Ciliary Dyskinesia.
767 *Reprod Biol Endocrinol* **23**, 48 (2025).
768 38. Liang, Y. & Tedder, T. F. Identification of a CD20-, FcεRIβ-, and HTm4-Related Gene
769 Family: Sixteen New MS4A Family Members Expressed in Human and Mouse. *Genomics* **72**,
770 119–127 (2001).
771 39. Li, W. *et al.* Sperm Associated Antigen 6 (SPAG6) Regulates Fibroblast Cell Growth,
772 Morphology, Migration and Ciliogenesis. *Sci Rep* **5**, 16506 (2015).
773 40. Teves, M. E. *et al.* Sperm-Associated Antigen 6 (SPAG6) Deficiency and Defects in
774 Ciliogenesis and Cilia Function: Polarity, Density, and Beat. *PLoS One* **9**, e107271 (2014).
775 41. Sapiro, R. *et al.* Male Infertility, Impaired Sperm Motility, and Hydrocephalus in Mice
776 Deficient in Sperm-Associated Antigen 6. *Mol Cell Biol* **22**, 6298–6305 (2002).
777 42. Kanie, T. *et al.* A hierarchical pathway for assembly of the distal appendages that organize
778 primary cilia. *eLife* **14**, e85999 (2025).
779 43. Radhakrishnan, P. *et al.* Biallelic Variants in Impair Ciliogenesis and Cause a Severe
780 Neurological Disorder. *Clinical Genetics* **107**, 311–322 (2025).

781 44. Liu, X., Peng, Y. & Wang, J. Integrative analysis of DNA methylation and gene expression
782 profiles identified potential breast cancer-specific diagnostic markers. *Bioscience Reports* **40**,
783 BSR20201053 (2020).
784 45. Lu, C. *et al.* Identification of hub genes in AR-induced tamoxifen resistance in breast cancer
785 based on weighted gene co-expression network analysis. *Breast Cancer Res Treat* **197**, 71–82
786 (2023).
787 46. Henriksson, S. *et al.* The scaffold protein WRAP53β orchestrates the ubiquitin response
788 critical for DNA double-strand break repair. *Genes Dev* **28**, 2726–2738 (2014).
789 47. Legrain, P. *et al.* The Human Proteome Project: Current State and Future Direction. *Mol Cell*
790 *Proteomics* **10**, M111.009993 (2011).
791 48. Kobayashi, A. *et al.* The Increase in the Frequency and Amplitude of the Beating of Isolated
792 Mouse Tracheal Cilia Reactivated by ATP and cAMP with Elevation in pH. *Int J Mol Sci* **25**,
793 8138 (2024).
794 49. Rosenbaum, J. L. & Witman, G. B. Intraflagellar transport. *Nat Rev Mol Cell Biol* **3**, 813–825
795 (2002).
796 50. Hildebrandt, F., Benzing, T. & Katsanis, N. Ciliopathies. *N Engl J Med* **364**, 1533–1543
797 (2011).
798
799
800
801
802
803
804
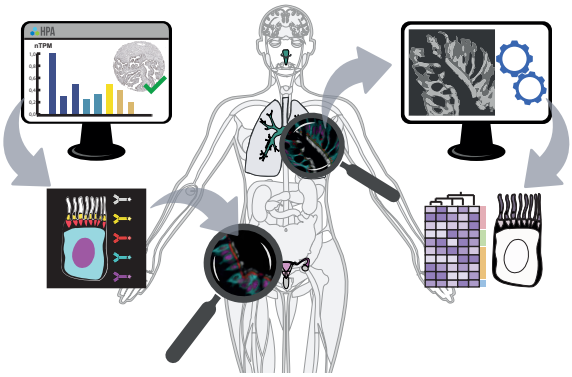
For TOC Only